JOURNAL OF BUILDING PHYSICS

Original Article

Journal of Building Physics
2015, Vol. 38(5) 389–418
© The Author(s) 2013
Reprints and permissions:
sagepub.co.uk/journalsPermissions.nav
DOI: 10.1177/1744259113506072
jen.sagepub.com
SAGE

Moisture transfer through the membrane of a cross-flow energy recovery ventilator: Measurement and simple data-driven modeling

CR Boardman and Samuel V Glass

Abstract

The moisture transfer effectiveness (or latent effectiveness) of a cross-flow, membrane-based energy recovery ventilator is measured and modeled. Analysis of in situ measurements for a full year shows that energy recovery ventilator latent effectiveness increases with increasing average relative humidity and surprisingly increases with decreasing average temperature. A simple finite difference heat and moisture transfer model is developed, which can explain these results and predict energy recovery ventilator latent effectiveness based on simplified physics and material properties. The model parameters are discussed and, in the case of the membrane's moisture sorption curve and moisture permeability, compared to direct laboratory measurements.

Keywords

Energy recovery ventilator, moisture transfer effectiveness, indoor air quality, sorption isotherm, moisture transfer model, membrane, permeability, moisture diffusion

Introduction

Mechanical ventilation is essential in high-performance residential buildings. ASHRAE Standard 62.2 (ASHRAE, 2010) spells out the widely accepted

Forest Products Laboratory, U.S. Forest Service, Madison, WI, USA

Corresponding author:

CR Boardman, Forest Products Laboratory, U.S. Forest Service, 1 Gifford Pinchot Dr., Madison, WI 53726, USA.

Email: cboardman@fs.fed.us

residential standard for acceptable indoor air quality and includes supply, exhaust, and balanced ventilation. The use of heat or energy recovery to condition the fresh air needed for ventilation is increasingly common in airtight houses. A variety of techniques, such as fixed plates or rotary heat wheels, are used to transfer heat between supply and exhaust air (ASHRAE, 2012; Besant and Simonson, 2003). But ventilation also affects building durability and occupant comfort through changes in indoor humidity (Barringer and McCugan, 1989; Fang et al., 2011; Walker and Sherman, 2007).

Building designers can use a wide variety of well-developed energy models to gain insight into the energy performance implications of different design options. But with the overall reduction in building energy use, increased attention should be given to understanding moisture transfer to ensure both durability and comfort. Heat, air, and moisture (HAM) models can be used to give insight into moisture movement with the goal of improving building durability. These HAM models rely on material properties and simplified building physics to calculate both heat and moisture transfer within buildings, often with a focus on the envelope. Whole-building HAM is under active development with recent work done as part of IEA Annex 41 (Rode and Woloszyn, 2007). The mechanical system designer focused on occupant comfort has fewer resources directly available for calculating the effects on heating, cooling, and dehumidification loads from water vapor transfer in an energy recovery ventilator (ERV) core. Most of the background work on moisture transfer effectiveness was done to aid ERV designers (Niu and Zhang, 2001; Sparrow et al., 2001; Tanaka, 1984; Zhang and Jiang, 1999). However, the Home Ventilating Institute (HVI) does publish heat and moisture transfer effectiveness numbers for certified ERV products, as described in the "Measurement results and analysis" section of the HVI Certified Products Directory (HVI, 2012). These numbers are based on CAN/CSA-C439, *Standard Laboratory Methods of Test for Rating the Performance of Heat/Energy-Recovery Ventilators*, and typically give whole-unit efficiency metrics for winter and summer design conditions (CSA, 2009). This article aims to extend the understanding of moisture transfer effectiveness over a broader range of conditions. Thus, it will present some moisture transfer models for a cross-flow, membrane-based ERV with the goal of providing useful equations for calculation and insight into the key variables that determine ERV moisture transfer.

The need for this kind of ERV modeling became clear during an earlier investigation (Boardman et al., 2010), in which all the moisture flows into and out of a house were calculated over several seasons, including mechanical ventilation with the ERV. Because published effectiveness data were limited, in situ measurements were made with temperature and humidity sensors and presented as a simple correlation of ERV moisture transfer effectiveness with average relative humidity (RH). The moisture transfer effectiveness (or latent effectiveness), ε, is defined as the ratio of the actual transfer of moisture to the maximum possible transfer of moisture between airstreams (ASHRAE, 2012). This article uses the previous data, extends it to include over 1 year of measured in situ ERV moisture transfer effectiveness,

and adds independent laboratory testing of the same ERV. This data set is used to improve the correlation and to calibrate more detailed moisture transfer models for this type of water vapor–permeable plate cross-flow ERV. While the results are specific to the ERV in the case study, the models developed could be useful for any permeable plate cross-flow ERV.

Review of ERV geometry and moisture transfer effectiveness

A schematic representation of the ERV core is presented in Figure 1, along with a numbering scheme for four ports. Port 1 is the outside air inlet, Port 2 is the outlet for conditioned supply air to the building, while Port 3 is the return air inlet (used to condition the incoming air), and Port 4 is the exhaust air outlet.

In most installations, Port 2, the supply air, is connected to a heating, ventilation, and air-conditioning (HVAC) system, as was done for this study. If the supply and exhaust dry air mass flow rates are equal, then the effectiveness can be expressed simply in terms of the humidity ratios, w (the ratio of the mass of water vapor to the mass of dry air), of the airstreams as shown in Figure 1

$$\varepsilon = \frac{w_1 - w_2}{w_1 - w_3} \tag{1}$$

The moisture transfer effectiveness of the ERV used in this study ranged from 19% to 61% during normal use over 12 months of operation. Our aim is to better

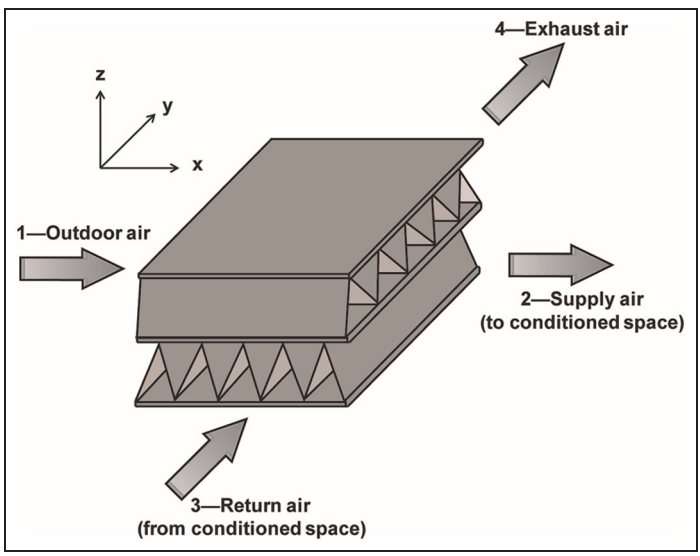

Figure 1. Simplified schematic representation of cross-flow ERV core showing ports, airflow directions, spacer plates forming air channels, and membrane.
ERV: energy recovery ventilator.

understand what variables control this large range. We use a data-driven modeling approach and first review the data sources that help to validate the models that are presented later.

Experimental methods and materials

ERV moisture transfer effectiveness

The primary data set comes from measurement of RH (h) and temperature (t) using probes placed in each inlet and outlet duct of the ERV. The probe placement for the outlet ducts was far enough after exit from the ERV core so that the air could reasonably be assumed to be well mixed. The ERV was used in the Research and Demonstration House on the campus of the US Department of Agriculture (USDA) Forest Service (FS) Forest Products Laboratory in Madison, WI (Boardman et al., 2010). Sensor values were recorded each minute and collected for a full year during which interior conditions were maintained for human comfort although no one lives in the house. The temperature and humidity probes had measurement errors of $\pm 0.1\,°C$ and ± 0.008 in fractional RH when near our room temperature conditions, increasing to $\pm 0.2\,°C$ and ± 0.013 fractional RH at $0\,°C$. The ERV ran for 40 min in each 2-h cycle, and a steady-state condition was achieved after about 6 min. In this study, the air flows into and out of the house were roughly balanced, and ERV steady-state operation was defined as when the two moisture mass flows were within 4% of each other. The humidity ratios and moisture transfer effectiveness were calculated for each minute, and the overall moisture transfer effectiveness for each operation period was calculated as the average of all minutes after steady state had been achieved. No other ERV operational control strategies were used, so that the ERV often ran even when the indoor and outdoor conditions were similar. Under these conditions, there is a large uncertainty in the effectiveness. Results with uncertainty greater than 40% were excluded from the data set. The airflow rate was measured periodically over the course of the study using two methods. The primary method was to calculate the effect of the ERV by measuring the overall air exchange rate for the house using tracer gas decay, with and without the ERV operating. A detailed air infiltration model, accounting for leakage, wind, and stack effects on air infiltration, was calibrated using the tracer gas measurements under both operational conditions (Boardman et al., 2010). The ERV airflow rate was thus estimated to be $53 \pm 5\ L\ s^{-1}$. The secondary method was to check the airflow in the supply duct to the house using a vane anemometer that gave consistent values. The flow was known to be roughly balanced from previous extensive studies of the HVAC system (Carll et al., 2010).

To supplement the primary data set with extreme conditions not seen in a typical installation, the ERV was sent to an outside laboratory capable of certifying ERV performance for the HVI. Again sensors in each duct measured h and t each minute. Eight different conditions were monitored in the laboratory, and average

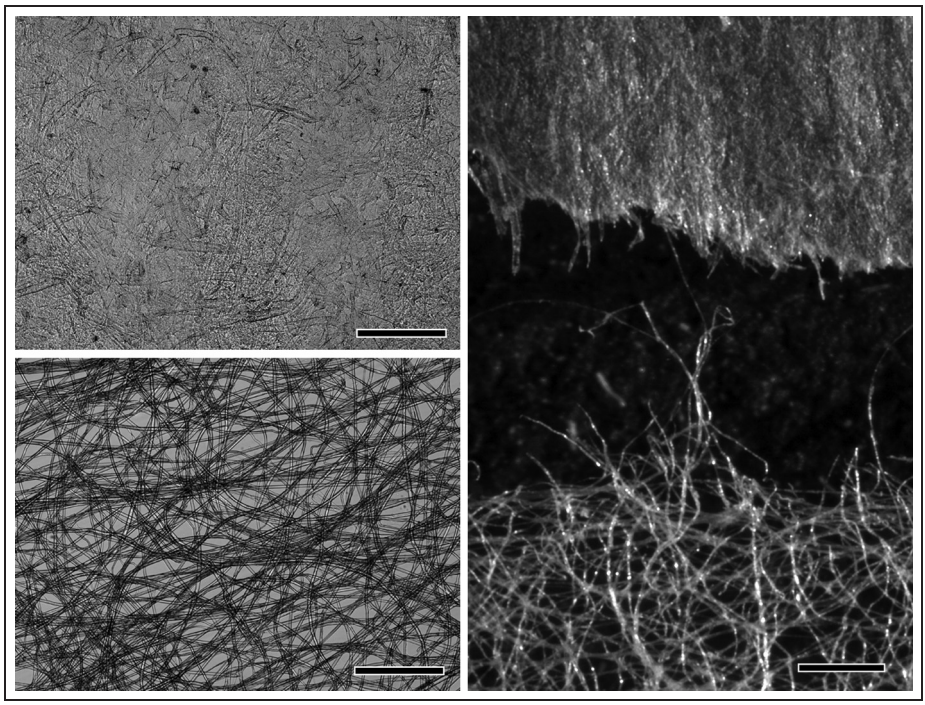

Figure 2. Transmitted light micrographs (scale bars = 400 μm) of the ERV membrane (top left) and ordinary lens tissue (bottom left) illustrating higher bulk density and lower bulk density cellulosic materials. Stereomicrographs of the same materials (top right and bottom right, respectively, scale bar = 500 μm) with torn edges to show differences in fiber characteristics between the two materials.
ERV: energy recovery ventilator.

latent effectiveness calculated after steady-state conditions were achieved. The target airflow through the ERV unit in the laboratory was 57.6 L s^{-1} with actual measured values of 56 ± 2 L s^{-1} balanced flow. The airflow in the laboratory was thus slightly faster than that for our primary data set, resulting in slightly lower overall moisture transfer effectiveness. This allowed us to do limited modeling of the effects of airflow speed, but our main interest was the effect of different temperature and humidity conditions. No systematic attempt was made to test different airflow speeds although this clearly influences moisture transfer effectiveness of the core.

ERV membrane general properties

This section provides a brief overview of the basic material properties of the cellulosic membrane that makes up the ERV core. Figure 2 shows transmitted light micrographs and a stereomicrograph of the ERV membrane compared with lens tissue

paper, illustrating the close spacing of the organic components of the ERV membrane, which impede gas flow. Membrane thickness is 20 μm with dry density of 1060 kg m^{-3}, which is less than cellulose at approximately 1500 kg m^{-3}.

ERV membrane hygric properties

In addition to the overall effectiveness of the ERV unit, we investigated two material properties of the ERV membrane, again focused on the effects of different h and t. We measured the moisture sorption isotherm at 0%–95% RH at 10 °C, 25 °C, and 40 °C by placing a small sample of ERV membrane fragments (totaling ~5 mg dry mass) in a gravimetric vapor sorption apparatus (IGAsorp; Hiden Isochema, Warrington, UK). The instrument includes a microbalance with a resolution of 0.1 μg. The sample is placed in a temperature-controlled chamber through which flows a nitrogen stream with controlled humidity, generated by mixing dry and saturated nitrogen streams using electronic mass flow controllers. The moisture content of the sample was determined after reaching equilibrium at each condition (or sufficiently close to equilibrium that the equilibrium value could be determined by extrapolation from the time-dependent sorption response). The membrane fragments were cut out of an ERV core of the same type as the one used in our unit, with care taken to avoid including structural spacer plates, which form the channels in the ERV core. The dry mass of the membrane was measured after all the data had been collected (so as not to change its native hygroscopicity by drying it at high temperature prior to measurements). The stable dry mass was determined under flow of dry nitrogen with the sample temperature brought to 105 °C. Assuming that the membrane does not contain volatile compounds other than water, moisture content determinations with this method have a measurement error of less than 0.001 kg kg^{-1}.

Additionally, a permeation cell accessory allows the instrument to be used for measuring water vapor transmission through a material. This cell is essentially a diffusion cup in miniature, with an inner diameter of 12 mm. A saturated salt solution ($MgCl_2$ or NaCl) was placed inside the cell, and multiple layers of ERV membrane (between three and seven layers) were sealed to the cell above the solution. The samples had some remnants of the structural spacer plates and glue lines used to create the core. The permeation cell assembly was placed in the instrument, suspended from the microbalance to measure the mass loss or gain due to a vapor pressure difference between the moist nitrogen stream and the saturated salt solution. Experiments were done at 25 °C over a range of RH conditions, with average RH between about 20% and 80%. Error analysis for the measured moisture permeability of the ERV membrane is described in Appendix 2. In this article, we use the term "permeability" to refer to the coefficient for moisture transfer when vapor pressure is the driving potential. We use "vapor permeability" exclusively for vapor diffusion and "moisture permeability" generally for combined vapor and bound water diffusion.

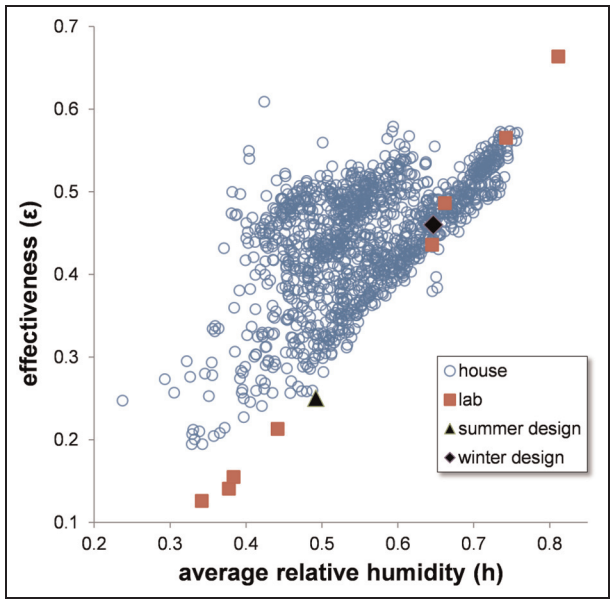

Figure 3. Moisture transfer effectiveness versus average relative humidity.

Measurement results and analysis

ERV moisture transfer effectiveness

The basic trend, as illustrated in Figure 3, was that ERV moisture transfer effectiveness ε increased with the average RH (average of h from Port 3—inside and Port 1—outside). This was an expected result since the effectiveness should increase with better moisture transfer across the membrane. The membrane moisture permeability was expected to increase with increasing RH, as is often the case with common hygroscopic building materials (Straube and Burnett, 2005). The results from the test laboratory had slightly lower overall effectiveness and clearly show the same trend. The ERV airflow in the laboratory was slightly higher than in the house as noted previously. Moisture transfer effectiveness typically decreases as airflow increases (ASHRAE, 2012; Barringer and McCugan, 1989; Tanaka, 1984), which can explain why the laboratory values are slightly lower than the typical house data. Figure 3 also shows the HVI-published moisture transfer effectiveness for winter and summer design conditions for this particular ERV. This shows that both the laboratory and house data track with the published figures. However, factors other than RH and airflow clearly influence moisture transfer in the ERV core. In the previous investigation (Boardman et al., 2010), we fit a subset of these data to an exponential function using two fit parameters along with the average RH $\bar{h}$

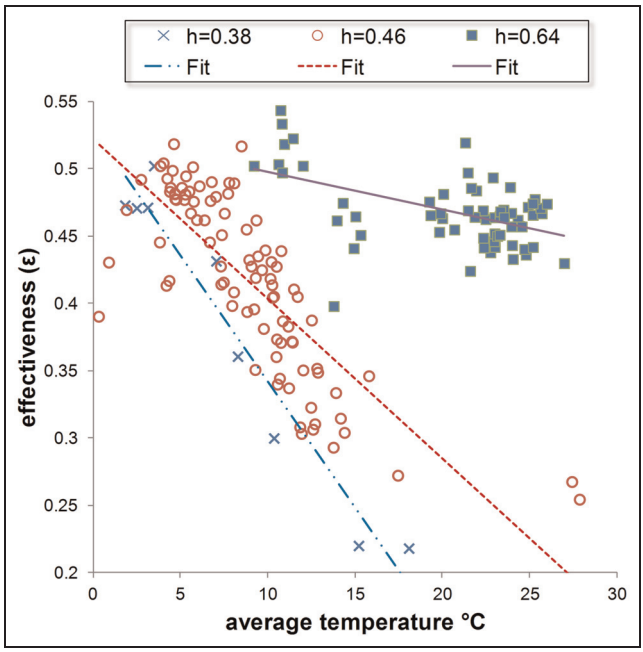

Figure 4. Moisture transfer effectiveness versus average temperature at select constant average relative humidities.

and average temperature $\bar{T}$ (K), the averages taken between indoor and outdoor conditions

$$\varepsilon = \alpha_2 \exp\left(\beta_2 \frac{\bar{h}}{\bar{T}}\right) \tag{2}$$

where the fit parameters are $\alpha_2 = 0.178$ and $\beta_2 = 4.88$ K.

However, a better fit can be achieved if careful attention is paid to how the temperature influenced the effectiveness. Specifically, when the humidity was high, the temperature had little effect, but when $\bar{h}$ was low the temperature had greater effect, in that lower $\bar{t}$ gave higher effectiveness. These trends are illustrated in Figures 4 and 5 in which select subsets of the house data are plotted. In Figure 4, points with constant $\bar{h}$ are plotted against $\bar{t}$, while in Figure 5 points with constant $\bar{t}$ are plotted against $\bar{h}$.

Figure 5 shows the expected result that effectiveness increases with $\bar{h}$, as noted in the discussion of Figure 3. However, the effect was less strong at low temperatures, and Figure 4 shows that temperature had a large influence on effectiveness at low RH levels. Perhaps unexpectedly, the effectiveness increased with decreasing

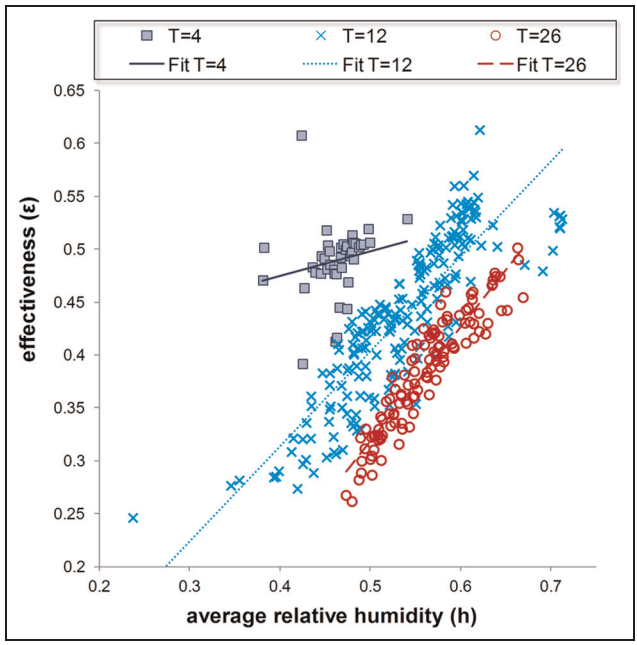

Figure 5. Moisture transfer effectiveness versus average relative humidity at select constant average temperatures.

temperature. With this insight about temperature effects in mind, we devised a better empirical form for fitting the data

$$\varepsilon = \alpha_3 \bar{h} + \beta_3 \bar{h}^2 + \gamma_3 \bar{t}(\bar{h} - 1) \tag{3}$$

Here, the empirical fit parameters are $\alpha_3 = 1.464$, $\beta_3 = -0.836$, and $\gamma_3 = 0.01692\,°\mathrm{C}^{-1}$; $\bar{t}$ is the average temperature in °C. This polynomial form can predict the actual moisture transfer effectiveness with 50% less root-mean-squared error (RMSE) than the exponential model used previously (equation (2)). Figure 6 illustrates the improvement in prediction by plotting the predicted ε against the measured ε. Data points in perfect agreement would fall on the center line. The dotted line indicates the fit to ε predicted by the previous exponential model (data points not shown), which is worse than the dashed line that shows the fit using equation (3).

In summary, the moisture transfer effectiveness increased with increased average RH but decreased with increased average temperature. The temperature effect may not be intuitive, but both trends are in agreement with the predictions from a detailed heat and moisture transfer model of a cross-flow air-to-air enthalpy exchanger presented by Niu and Zhang (2001). Their key result was to characterize the moisture movement through the membrane using a resistance model as the

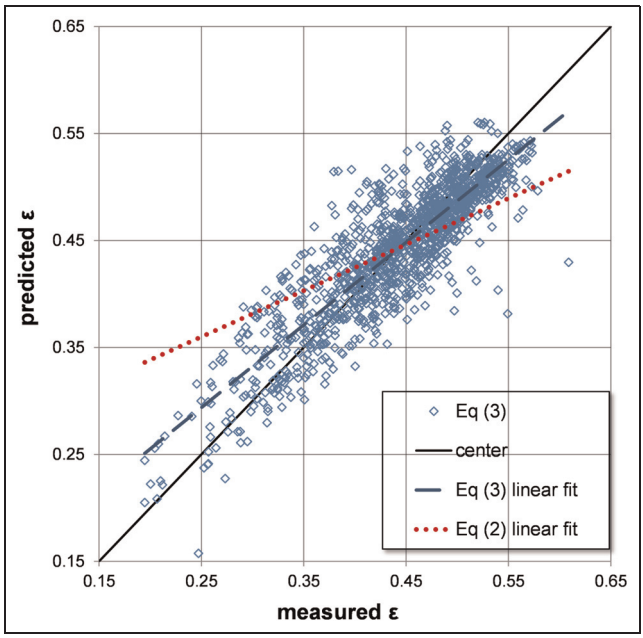

Figure 6. Predicted versus measured moisture transfer effectiveness.

combination of the resistance of the boundary layer air near the membrane surface and the resistance of the membrane material itself, which varied with temperature and humidity. Our model developed later is both a simplification and refinement of their model, so before proceeding further it will be useful to outline the Niu and Zhang model, specifically to highlight the basic driving forces and show how the temperature dependence arises.

Model of Niu and Zhang (2001)

The driving force for moisture transport is the gradient in moisture content u across the membrane. Steady-state moisture flux is modeled with Fick's law, and the moisture conductivity constant D_u is assumed to be independent of moisture content and temperature

$$J_m = -D_u \frac{\partial u}{\partial z} \tag{4}$$

A number of transformations are needed to relate moisture flow to effectiveness, which is expressed in terms of the difference in humidity ratio between the supply and exhaust airstreams. To accomplish this, they first relate the membrane moisture content to RH

$$J_m = -D_u \frac{\partial u}{\partial h}\frac{\partial h}{\partial z}$$

where $\partial u/\partial h$ is the slope of the sorption isotherm, which is assumed to be independent of temperature. Then, they relate the RH to the humidity ratio so that moisture flow can be expressed as

$$J_m = -D_u \frac{\partial u}{\partial h}\frac{\partial h}{\partial w}\frac{\partial w}{\partial z} \tag{5}$$

Assuming the ideal gas law, humidity ratio is given by $w = 0.621945\,(p_v/(P_{atm} - p_v))$, which can be reasonably approximated (typically within a few percent) by

$$w = 0.622\left(\frac{p_v}{P_{atm}}\right) = 0.622\left(\frac{hp_s}{P_{atm}}\right) \tag{6}$$

The dependence of the saturation vapor pressure of water on temperature is often approximated as an exponential and given as an acceptable solution to the Clausius-Claperyron equation in the form

$$p_s = \alpha_7 \exp\left(-\frac{L}{R_v T}\right) \tag{7}$$

where α_7 is an integration constant. We will use a more rigorous form for p_s in the simple model developed later. Niu and Zhang apparently set the constants in equation (7) at 298 K, where the ratio of the enthalpy of vaporization of water to the specific gas constant for water vapor is $L/R_v = 5294$ K, and the integration constant is $\alpha_7 = 1.63 \times 10^{11}$ Pa. Combining equations (6) and (7) and assuming standard atmospheric pressure ($P_{atm} = 101{,}325$ Pa) gives

$$\frac{h}{w} = \frac{e^{5294/T}}{10^6} \tag{8}$$

Finally, Niu and Zhang express the moisture flow across the membrane thickness d in terms of the humidity ratio difference Δw between the two surfaces of the membrane in contact with supply and exhaust airstreams (combining equations (5) and (8))

$$J_m = \frac{D_u}{d}\left(\frac{1}{\psi}\right)\Delta w \text{ with } \psi^{-1} = \left(\frac{\partial u}{\partial h}\right)\left(\frac{e^{5294/T}}{10^6}\right) \tag{9}$$

We can now see how the temperature dependence enters the equation, namely, through the saturation vapor pressure approximation. Niu and Zhang define ψ in equation (9) as the coefficient of moisture diffusion resistance (CMDR), which determines how the membrane diffusion resistance depends on the driving

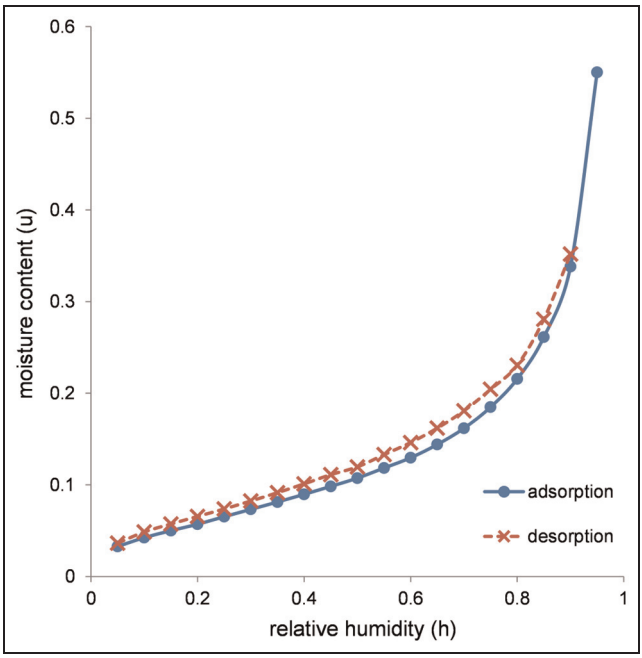

Figure 7. ERV membrane adsorption and desorption isotherms at 25 °C.
ERV: energy recovery ventilator.

conditions. To make further progress, we must now explore the sorption isotherm since its derivative has an effect on the resistance to moisture flow. We present our moisture sorption measurements for the ERV membrane and two ways of fitting the data.

Membrane sorption isotherms

The ERV membrane is a proprietary cellulosic sheet that allows transfer of heat and moisture in the ERV core but is relatively impermeable to air and pollutant transfer. Its Type II moisture sorption isotherm is similar to that of other cellulosic materials, which typically exhibit hysteresis. That is, the gravimetric moisture content (u = mass of water/mass of dry sample) is typically higher when equilibrium is reached from desorption than when it is reached from adsorption. Figure 7 illustrates these effects for ERV membrane isotherms at 25 °C. Since sorption hysteresis is relatively small, we neglect it and take the average of the adsorption and desorption curves. Average u values are presented in Figure 8 for three temperature conditions, along with the fit to a modified Oswin equation (Chen and Morey, 1989; Oswin, 1946) of the form

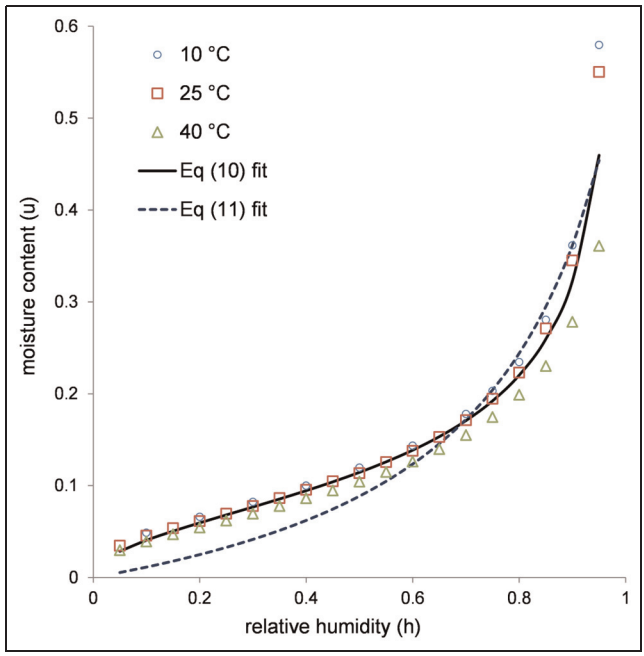

Figure 8. ERV membrane sorption data (average of adsorption and desorption) at three temperatures along with curve fit to equation (10) at 25 °C and curve fit to equation (11) which is independent of temperature.
ERV: energy recovery ventilator.

$$u = (\alpha_{10} + \beta_{10}t)\left(\frac{h}{1-h}\right)^{\gamma_{10}} \tag{10}$$

where the empirical fit parameters are $\alpha_{10} = 0.133$ kg kg^{-1}, $\beta_{10} = -0.00074$ kg kg^{-1} °C^{-1}, and $\gamma_{10} = 0.472$.

While we prefer the modified Oswin form for describing the sorption isotherm, we also fit the data to equation (11) as presented by Niu and Zhang (2001) so that we could compare our data to their model

$$u = \frac{u_{\max}}{1 - C + C/h} \tag{11}$$

where $C = 5.65$ is a shape parameter and $u_{max} = 0.589$ kg kg^{-1} is the moisture content extrapolated to 100% RH ($h = 1$). Since this form does not include a temperature term, the fit was optimized to give the best C and u_{max} across all the three moisture sorption isotherms. This fit is also shown in Figure 8 as the dashed curve.

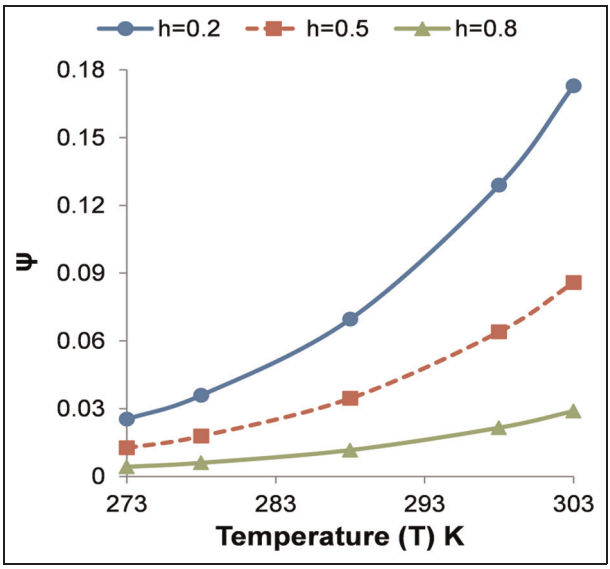

Figure 9. CMDR versus temperature.
CMDR: coefficient of moisture diffusion resistance.

Discussion of model of Niu and Zhang

We can now understand the form of the CMDR (ψ, see equation (9)) and thus explain the factors controlling moisture transfer across the ERV membrane. Taking the partial derivative of moisture content with respect to RH in equation (11), Niu and Zhang (2001) express the dimensionless ψ as follows

$$\psi = \frac{10^6(1 - C + C/h)^2 h^2}{e^{(5294/T)} u_{\max} C} \tag{12}$$

With our values of C and u_{max}, ψ increases modestly with increasing temperature but decreases significantly with increasing humidity, as illustrated in Figures 9 and 10.

The humidity sensitivity in the model of Niu and Zhang enters when the moisture content gradient across the membrane is transformed into an RH gradient, by way of the derivative of the sorption curve $\partial u/\partial h$ (recall that the moisture conductivity coefficient D_u is assumed to be constant). Intuitively, it makes sense that ψ decreases significantly with increasing humidity given that the sorption curve increases sharply at higher h. Imagine two conditions with the same T, the same Δw, the same Δh, but different average h. For the higher average RH condition, the actual driving force is larger than for the lower average RH condition because the moisture content difference Δu between the two sides of the membrane is larger given the sharp increase in u with increasing h.

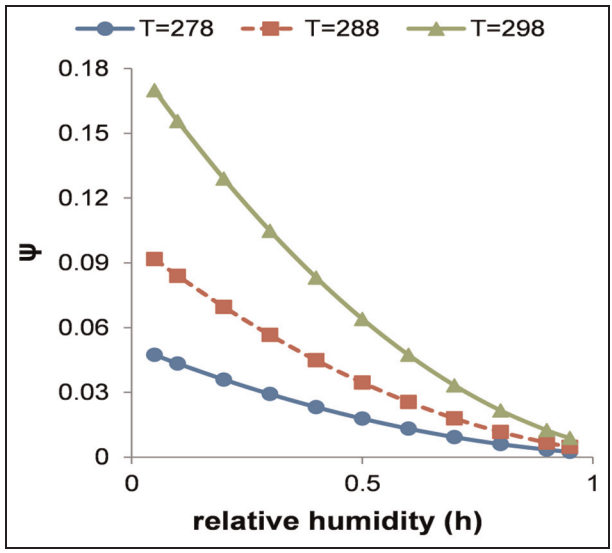

Figure 10. CMDR versus relative humidity.
CMDR: coefficient of moisture diffusion resistance.

The exponential dependence on the temperature enters when Niu and Zhang transform the RH to the humidity ratio, which requires an expression for the saturation vapor pressure. The counter-intuitive temperature result now makes sense given that the humidity ratio w is used to define the effectiveness, and the CMDR is defined in relation to w, but the ultimate mass transfer is driven by the moisture content difference across the membrane. Imagine two different temperature conditions with the same average RH and the same Δw. The lower temperature condition will have a higher RH difference Δh, and hence a higher moisture content difference Δu across the membrane, leading to a higher driving force and hence higher effectiveness.

The Niu and Zhang model is useful for laying out the basic physical mechanisms governing heat and moisture transfer in a cross-flow ERV. Our model developed below shares many assumptions with the Niu and Zhang model, but makes a few refinements that are common when modeling heat and moisture transfer in cellulosic materials. We first discuss assumptions related to moisture transfer through the membrane. Niu and Zhang assume a constant moisture conductivity coefficient. In contrast, our model recognizes two potential diffusion mechanisms, namely, water vapor diffusion and bound water diffusion (Stamm, 1964). We model vapor diffusion as dependent on temperature and bound water diffusion as dependent on both temperature and moisture content. Both models assume that the sorption of water vapor by the membrane is in equilibrium, and both neglect sorption hysteresis. While Niu and Zhang use only the adsorption isotherm and neglect the effect of

temperature, we take the average of the adsorption and desorption curves and account for temperature dependence as shown previously in Figure 8. Both models neglect hygroexpansion of the membrane.

Model development

Membrane moisture transfer model

We assume that the total moisture flux through the membrane (z-direction) is the sum of both vapor and bound water transport paths occurring in parallel: $J_m = J_v + J_b$. Furthermore, each path is assumed to follow Fick's first law. We show later that vapor diffusion is negligible at high RHs and perhaps also in general as was assumed by Niu and Zhang.

The water vapor flux $J_v = -D_v(\partial c_v/\partial z)$ is transformed such that the water vapor pressure gradient is the driving potential. Using the ideal gas equation, $c_v = p_v/R_vT$, and the relation $D_v = D_{va}(\varphi/\tau)$ between diffusivity of water vapor in the material D_v and diffusivity of water vapor in air D_{va}, we have $J_v = -(D_{va}\varphi/R_vT\tau)(\partial p_v/\partial z)$. Here, we can estimate the porosity, $\varphi = 0.32$, based on the apparent membrane density, but we do not know the tortuosity, τ, which accounts for the increased flow path for diffusion in a porous medium. We thus treat τ as a fitting constant. Finally, we express D_{va} by the empirical equation of Schirmer (1938): $D_{va} = 2.306\times10^{-5}(P_0/P_{atm})(T/273.15)^{1.81}$. Combining these equations we have

$$J_v = -\delta_v \frac{\partial p_v}{\partial z}, \text{where } \delta_v = 1.94\times10^{-7}\frac{T^{0.81}\varphi}{P_{atm}\tau} \tag{13}$$

The bound water flux is driven by the gradient in bound water concentration: $J_b = -D_b(\partial c_b/\partial z)$. This equation is transformed in several steps to make vapor pressure gradient the driving potential. We express bound water concentration in terms of moisture content ($c_b = \rho_0 u$) and relate moisture content to RH: $J_b = -\rho_0 D_b(\partial u/\partial h)(\partial h/\partial z)$. RH by definition is $h = p_v/p_s$. Neglecting any thermal gradient across the membrane (so that saturation vapor pressure is constant) gives $\partial h/\partial z = (1/p_s)(\partial p_v/\partial z)$. As discussed below, the thermal resistance of the membrane is small relative to boundary layer resistances, so thermal gradients across the membrane are minimal. Furthermore, we are neglecting any thermal diffusion which we expect to be small (Janssen, 2011). Thus, we have

$$J_b = -\delta_b \frac{\partial p_v}{\partial z}, \text{where } \delta_b = \frac{\rho_0 D_b}{p_s}\frac{\partial u}{\partial h} \tag{14}$$

Finally, we use models for the bound water diffusion coefficient D_b and saturation vapor pressure p_s to arrive at the full expression for δ_b. We assume that bound water diffusion across the membrane is an activated process, where the activation

energy depends on moisture content, as given by Siau (1995) for bound water diffusion in wood in the transverse directions (across the grain)

$$D_b = D_0 \exp\left(-\frac{E_b}{RT}\right), \text{with } E_b = 38,500 - 29,000u \tag{15}$$

We choose to make D_0 an adjustable parameter in our model, but compare our result with direct measurements of the total diffusivity of the membrane. Finally, we use the following expression for p_s, given by Koutsoyiannis (2012)

$$p_s = p_0 \exp\left[24.921\left(1 - \frac{T_0}{T}\right)\right]\left(\frac{T_0}{T}\right)^{5.06}, \text{with } T_0 = 273.16, \mathrm{K}, p_0 = 611.657, \mathrm{Pa} \tag{16}$$

We thus have two fitting parameters for moisture transfer through the membrane, the tortuosity τ for vapor diffusion and the bound water diffusion parameter D_0. We optimize these parameters using our measured values of ERV heat and moisture transfer effectiveness as discussed below.

Finite difference model for ERV heat and moisture transfer

To gain further insight into the physical mechanisms that affect heat and moisture transfer in the ERV core, we developed a steady-state finite difference model. The geometry of the ERV core is depicted in Figure 1. The outdoor/supply airflow is in the x-direction, and the return/exhaust airflow is in the y-direction. Relevant geometric parameters of the ERV core and properties of the membrane are given in Table 1.

The finite difference model calculates temperature and humidity (both RH and water vapor pressure) at each node on the x–y grid, approximating the solution to the full differential equations. Although our membrane moisture transfer model is more refined than that of Niu and Zhang, we wanted to make the finite difference model as simple as possible. Our model takes the temperature and humidity condition of the outdoor and return airstreams and calculates the condition of the supply and exhaust airstreams (see Figure 1). In the z-direction, each location in the x–y

Table 1. Parameters of the cross-flow membrane-based energy recovery ventilator.

Parameter	Symbol	Value
Length of supply channel	l	267 mm
Width of supply channel	Δy	3.5 mm
Average channel height	Δz	2 mm
Membrane thickness	d	20 μm
Membrane dry density	ρ_0	1060 kg m^{-3}

grid has three "resistors" that impede heat and moisture transfer from the incoming airstream to the outgoing airstream: two for the convective boundary layers on each side of the membrane and one for the membrane itself. Heat and moisture flows are tracked from each node to the next, in the supply and exhaust airflow directions as well as across the membrane.

For the sake of simplicity, we neglect heat conduction in the plane of the membrane (x- and y-directions). We assume that heat conduction and vapor diffusion in the airstreams are negligible compared to convective heat and mass transfer by bulk flow. This assumption is justified by Niu and Zhang (2001). Furthermore, we use a single air velocity for both supply and exhaust air flows and assume a constant specific heat capacity for air while allowing the density to vary with temperature but not pressure. These simplifying assumptions result in errors smaller than the uncertainty introduced by the base air velocity uncertainty of 10%. For example, even with these assumptions, there is typically a moisture mass balance between incoming and exhaust flows within 3% at steady-state conditions.

Heat transfer from the supply air through the membrane to the exhaust air (z-direction) depends on the difference in temperature and the total thermal resistance Z_h

$$q = \frac{T_{\text{supply}} - T_{\text{exhaust}}}{Z_h} \tag{17}$$

We initially assumed that the thermal conductivity of the membrane varies linearly with moisture content: $k = a + bu$. However, as discussed further below, the membrane thermal resistance is very small (<1%) compared to the boundary layer resistances, so this refinement is not significant. Because the thermal gradient across the membrane is minimal, we simply calculate the temperature at a given node in the membrane as the average of the airstreams on either side, and we neglect the heat of adsorption/desorption. The convective heat transfer coefficient h_h is assumed to increase linearly with air velocity: $h_h = A_h + B_h s$. This linear relationship is recommended by Straube and Burnett (2005) for low velocities. The total thermal resistance can then be expressed by

$$Z_h = \frac{2}{A_h + B_h s} + \frac{d}{k} \tag{18}$$

The equations for moisture transfer through the membrane (z-direction) are given above. Moisture flow is implemented in the finite difference model in a manner analogous to heat flow. Moisture transfer from the supply air through the membrane to the exhaust air depends on the difference in water vapor partial pressure p_v and the total moisture transfer resistance Z_m

$$J_m = \frac{p_{v,\,\text{supply}} - p_{v,\,\text{exhaust}}}{Z_m} \tag{19}$$

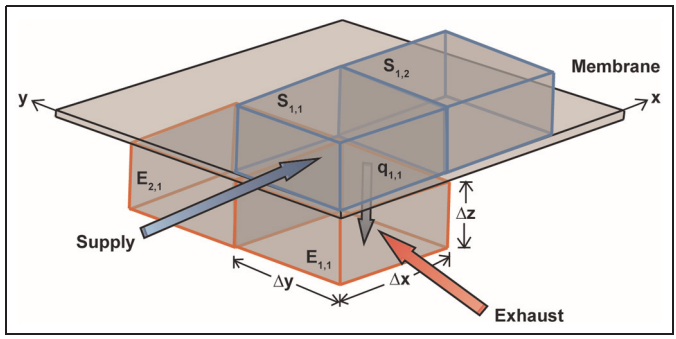

Figure 11. Grid layout with heat flows.

We assume that the convective mass transfer coefficient h_m increases linearly with air velocity: $h_m = A_m + B_m s$. Thus, the total moisture resistance is

$$Z_m = \frac{2}{A_m + B_m s} + \frac{d}{\delta_v + \delta_b} \tag{20}$$

Figure 11 depicts a two-dimensional numerical grid on the membrane at one corner of the ERV core.

The distances between nodes within the plane are Δx and Δy, with Δz being the equivalent channel height. The equivalent channel height of 2 mm refers to the height of a rectangular channel having the same cross-sectional area as the actual channel, whose shape is irregular. Peak channel height is 2.1 mm with approximately 95% of the channel open to flow; the rest is taken up by glue and spacer plates, thus $\Delta x/\Delta z$ is 134/(number of nodes). The outdoor/supply air (denoted S) flows above the membrane in the x-direction, and the return/exhaust air (denoted E) flows below the membrane in the y-direction. The boundary conditions are implemented such that the temperature and vapor pressure at all nodes $S_{i,1}$ are equal to T and p_v at the outdoor air inlet (Port 1), respectively; similarly, the temperature and vapor pressure at all nodes $E_{1,j}$ are equal to T and p_v at the return air inlet (Port 3), respectively.

Heat flows are considered first from the perspective of the supply side. Outdoor air flows into node $S_{1,1}$; some heat is transferred through the membrane to the exhaust side, and the rest flows into $S_{1,2}$. From the perspective of the exhaust side, room air flows into $E_{1,1}$, gains the heat that was transferred through the membrane from $S_{1,1}$, and flows into $E_{2,1}$. The heat flux $q_{1,1}$ through the membrane is calculated from equation (17). The temperature at $S_{1,2}$ is then calculated from energy balance, where we approximate $(\partial T/\partial x) \approx (T(S_{1,2}) - T(S_{1,1}))/\Delta x$. So

$$sA_x \rho c_p (T(S_{1,2}) - T(S_{1,1})) + 2qA_z = 0 \tag{21}$$

where the two different cross-sectional flow areas are $A_x = \Delta y \Delta z$ and $A_z = \Delta y \Delta x$.

The general expression for the supply side is

$$T(S_{i,j+1}) = T(S_{i,j}) - 2q_{i,j}\frac{\Delta x}{s\Delta z\rho c_p} \tag{22}$$

Similarly, for the exhaust side, we have

$$T(E_{i+1,j}) = T(E_{i,j}) + 2q_{i,j}\frac{\Delta x}{s\Delta z\rho c_p} \tag{23}$$

Moisture flows are analogous. Outdoor air flows into node $S_{1,1}$; some moisture is transferred through the membrane to the exhaust side, and the rest flows into $S_{1,2}$. From the perspective of the exhaust side, room air flows into $E_{1,1}$, gains the moisture that was transferred through the membrane from $S_{1,1}$, and flows into $E_{2,1}$. The moisture flux $J_{1,1}$ is calculated from equation (19). The vapor pressure at $S_{2,1}$ is then calculated using mass balance

$$\frac{sA_x}{R_vT}(p_v(S_{1,2}) - p_v(S_{1,1})) + 2J_m\alpha_{24}A_z = 0 \tag{24}$$

where we approximate $(\partial p_v/\partial x) \approx (p_v(S_{1,2}) - p_v(S_{1,1}))/\Delta x$. Note that the fit constant α_{24} is the fraction of the area available for moisture transport through the membrane. Some fraction of that area is not available because the channel is created with a thicker paper glued between membrane layers as a structural spacer. Approximately half the area is directly exposed to the membrane while much of the rest of the area is available for moisture transfer through the structural paper. The moisture transfer properties of the structural paper and glue could not be characterized. We set $\alpha_{24} = 0.95$ and found that with this setting, the model provides reasonable agreement with laboratory measurements of the membrane moisture permeability (shown later). In general, for the supply side, we have

$$p_v(S_{i,j+1}) = p_v(S_{i,j}) - 2J_{i,j}\alpha_{24}\frac{R_vT\Delta x}{s\Delta z} \tag{25}$$

where T is the temperature of the node $S_{i,j}$. Similarly, for the exhaust side, we have

$$p_v(E_{i+1,j}) = p_v(E_{i,j}) + 2J_{i,j}\alpha_{24}\frac{R_vT\Delta x}{s\Delta z} \tag{26}$$

At the outlet sides, we calculate values of temperature and vapor pressure as the average over the last n nodes ($S_{1,n}$ to $S_{n,n}$ for supply and $E_{n,1}$ to $E_{n,n}$ for return). We implemented this simple finite difference model in a spreadsheet. We found that a 100×100 grid was adequate and optimized the model parameters using the full data set, specifically comparing our model for membrane moisture transfer resistance to that of Niu and Zhang.

Table 2. Optimized parameters for the heat and moisture transfer model.

Parameter	Equation	Value
A_h	18	52 W m^{-2} K^{-1}
B_h	18	20 W s m^{-3} K^{-1}
k	18	0.1 W m^{-1} K^{-1}
A_m	20	0.4×10^{-6} kg m^{-2} s^{-1} Pa^{-1}
B_m	20	0.2×10^{-6} kg m^{-3} Pa^{-1}
τ	13	5×10^3
D_0	15	1.1×10^{-5} m^2 s^{-1}
D_u	9	5.6×10^{-9} kg m^{-1} s^{-1}

Modeling results and discussion

The optimized fit parameters are given in Table 2. At a typical air speed (s) of 2.2 m s^{-1}, these parameters show the total boundary layer thermal resistance (both sides) to be 0.021 m^2 K W^{-1}, while the membrane thermal resistance is only 0.0002 m^2 K W^{-1} or less than 1% of the total. This total thermal resistance is in the correct range. For example, if we assume fully developed laminar flow in the channels of the ERV, then the Nusselt number ($Nu = h_c d_c/k$, where h_c is the convective heat transfer coefficient) would be around 4 (like internal flow in a pipe). Thus, if the characteristic length (d_c) is 2 mm and assuming thermal conductivity (k) of air at 0.024 Wm^{-1}K^{-1}, then the resistance should be near 0.02 m^2 K W^{-1}. These results support the finding of Niu and Zhang that the thermal resistance is dominated by the boundary layer air and the thermal resistance of the membrane itself is negligible.

The optimized fit parameters for convective mass transfer show that at a typical air speed of 2.2 m s^{-1}, the total boundary layer moisture resistance (both sides) is 2.7×10^6 m^2 s Pa kg^{-1}. This moisture resistance is generally in the correct range. For example, if we assume the Lewis correlation between heat and mass transfer (see Incropera et al., 2006), we would predict a moisture resistance of 1.7×10^6 m^2 s Pa kg^{-1}.

Moisture transfer through the membrane was divided into water vapor diffusion and bound water diffusion, but the model optimization implies that it was dominated by bound water diffusion. The fit parameter that controls vapor diffusion is the tortuosity (τ from equation (13)). The model is not sensitive to changes in tortuosity, so there is a very large uncertainty in its value. On the basis of laboratory moisture permeability measurements at low RH (shown later), we set its value to 5×10^3 so that $\delta_v = 1 \times 10^{-14}$ kg m^{-1} s^{-1} Pa^{-1}. The fit parameter that controls the bound water diffusion is D_0 from equation (15) and has a value of 1.1×10^{-5} m^2 s^{-1} so that $\delta_b = 4.9 \times 10^{-13}$ kg m^{-1} s^{-1} Pa^{-1} at $h = 0.1$ and $T = 293$ K. Thus, the vapor diffusion is at most 3% of the bound water diffusion. This result supports the implicit assumption of Niu and Zhang that the water vapor diffusion through the membrane can be neglected. Figure 12 shows the variation in

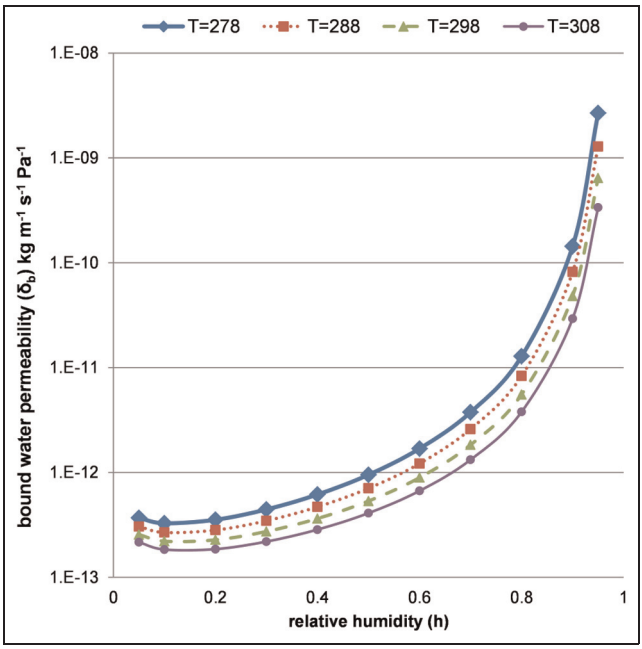

Figure 12. Bound water permeability versus relative humidity.

bound water diffusion with T and h, illustrating the dominance of this moisture transport mechanism especially at higher RH conditions.

The net result is a total moisture transfer resistance (both membrane and boundary layer air) of 35×10^6 m^2 s Pa kg^{-1} at $h = 0.5$ and $T = 293$ K. Only at the highest h does the air resistance become significant by setting a minimum resistance to moisture transfer. In fact, across the full range of RH, our resistance model yields values similar to those of Niu and Zhang. However, as Figure 13 illustrates, the shape of the curve is different primarily because our moisture resistance model includes a better fit for the sorption isotherm.

The modeling effort yields insight into the physical mechanisms that control heat and moisture transfer in the ERV core. For example, we confirmed that the heat transfer is completely controlled by the boundary layer air resistance, while the moisture transfer is dominated by the membrane moisture transfer resistance, as found by Niu and Zhang (2001) and Zhang and Jiang (1999). The model can also be used to understand the pattern of moisture flow across the surface of the membrane in a cross-flow ERV. For example, most of the action occurs at the leading edge of the membrane. Figure 14 shows the moisture flow through the membrane for the winter design condition.

However, if all you need is to predict the moisture transfer effectiveness, then equation (3) remains the simplest tool. Our model was able to achieve a slightly

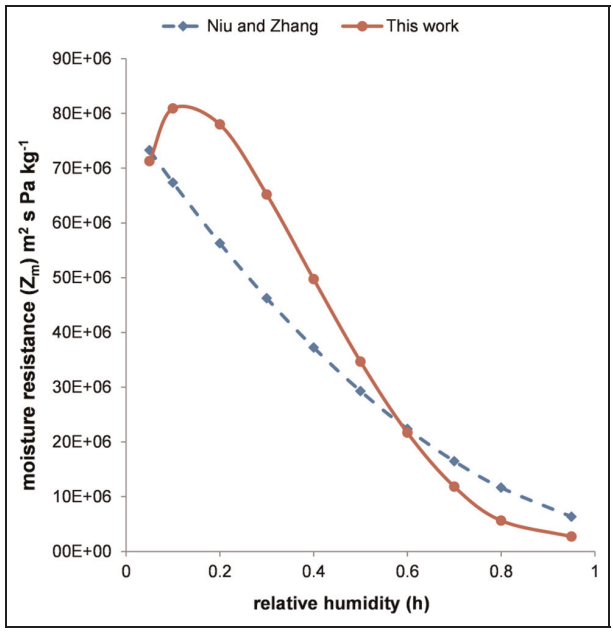

Figure 13. Membrane moisture transfer resistance versus relative humidity.

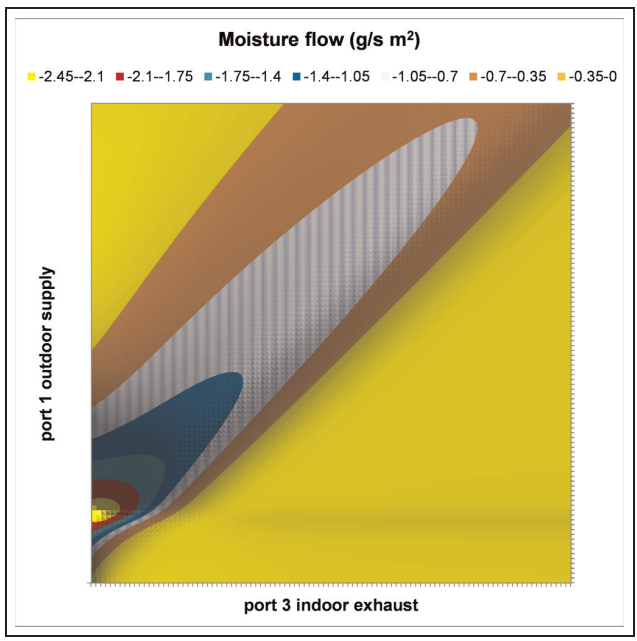

Figure 14. Illustration of moisture flow through membrane by location.

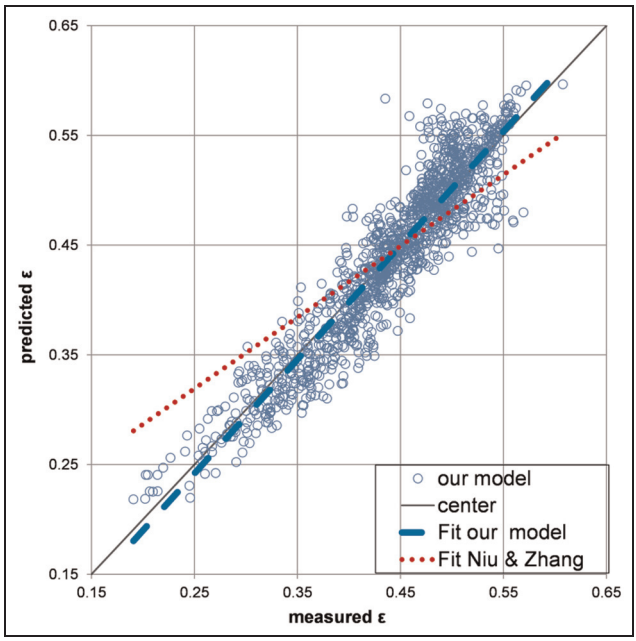

Figure 15. Model predictions versus measured effectiveness.

better RMSE when used to predict ε than the simple correlation, while the Niu and Zhang model had 74% more RMSE than equation (3). Figure 15 shows the predicted ε versus measured ε for both models. The significant difference between the models is that we allow the membrane diffusivity to vary with moisture content and temperature, similar to other wood-based materials. Both models were optimized for the best fit possible over the data set.

Finally, by comparison to laboratory measurements, we can see that our total membrane moisture permeability is in the correct range. The optimized diffusivity D_0 from equation (15) and fixed tortuosity value τ for equation (13) can be combined to create the total membrane permeability ($\delta_v + \delta_b$) and compared to measured values. As mentioned previously, we directly measured the total membrane permeability using the gravimetric vapor sorption apparatus. Figure 16 compares the measured data with the total permeability predicted by our model using parameters optimized to fit the in situ measured values of ERV moisture transfer effectiveness. There is good agreement at high RH and the trend is correct, but neither our model nor that of Niu and Zhang predicts the low permeability we measure at low RH.

Despite the overall success of our model, it still cannot capture all the variation in our data. Close inspection of Figure 15 reveals significant data scatter. To reduce the data clutter and see the trends more clearly, Figure 17 groups the data by

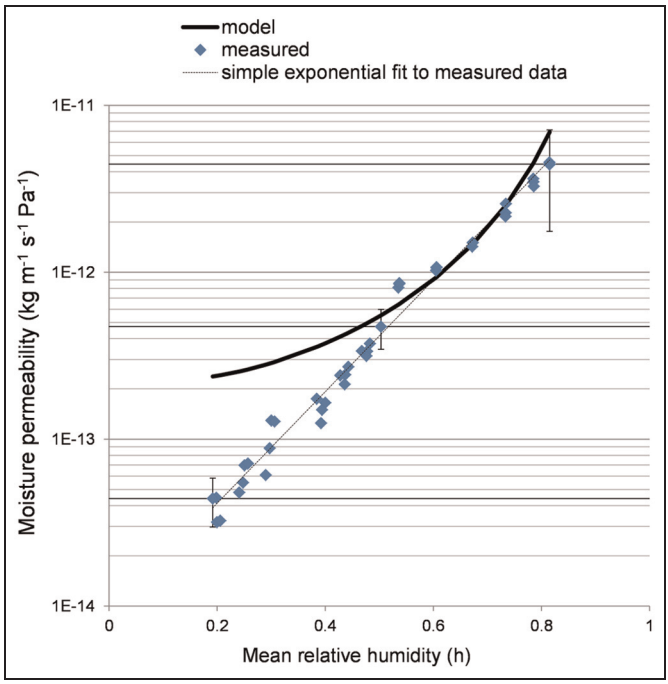

Figure 16. Measured membrane moisture permeability compared to optimized model. Error bars for select data points are based on analysis described in Appendix 2.

predicted value in bins and shows the average and standard deviation of the measured effectiveness for all data in each bin. The resulting average data points are best fit by a polynomial, which highlights that our predictions are too high for effectiveness above 50%. We can see a similar trend by inspecting the data outliers, those data points for which the prediction is outside the error bars for the measured data. The outlier data set and associated individual error bars are plotted in Figure 18.

There are no further obvious trends in the data outliers when examined for patterns in h or t, so it is not clear in which directions the model needs to be improved. There were no significant changes in ERV operation over the course of the year. We speculate that the model may be enhanced by further work on the bound water activation energy used in equation (15).

Conclusion

The large range in moisture transfer effectiveness for a water vapor–permeable membrane ERV can be accurately predicted by a simple polynomial such as equation (3), using average RH and temperature of the airstreams. The physical mechanisms that cause the effectiveness to increase at low temperature can be

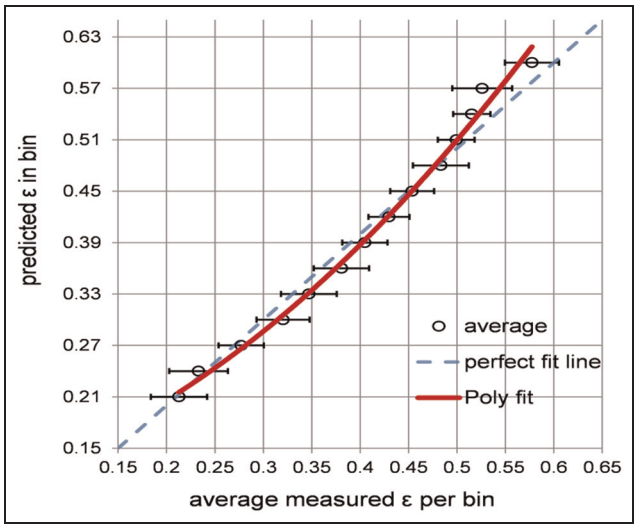

Figure 17. Predicted effectiveness in bins versus measured average and standard deviation for corresponding bin.

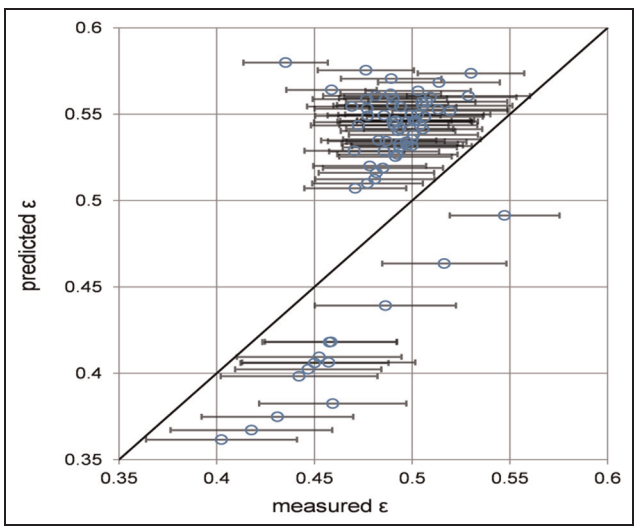

Figure 18. Predicted effectiveness data points outside the range of error bar for measurements.

understood by investigation of models based on simplified physics. These models can be used to predict effectiveness given reasonable material properties. The general models as developed should be useful for any cross-flow ERV with a

membrane core. The particular properties presented in this article were optimized for one ERV in field use and may prove useful for ERV designers and those concerned to understand the effects of ventilation on indoor humidity levels in high-performance residential buildings.

Acknowledgements

We thank Alex Wiedenhoeft of the Forest Products Laboratory for the micrographs in Figure 2. This article was improved by helpful comments from Jay Johnson (Professor emeritus, University of Washington) and three anonymous reviewers.

Funding

The authors acknowledge the support of the Forest Products Laboratory (FPL) in carrying out this work.

References

American Society of Heating, Refrigerating and Air Conditioning Engineers (ASHRAE) (2010) *ANSI/ASHRAE Standard 62.2, Ventilation for Acceptable Indoor Air Quality*. Atlanta, GA: American Society of Heating, Refrigerating and Air Conditioning Engineers.

American Society of Heating, Refrigerating and Air Conditioning Engineers (ASHRAE) (2012) Air-to-air energy recovery equipment. In: ASHRAE (ed.) *ASHRAE Handbook—HVAC Systems and Equipment*, ch. 26. Atlanta, GA: American Society of Heating, Refrigerating and Air Conditioning Engineers, pp. 26.1–26.28.

Barringer CG and McCugan CA (1989) Effect of residential air-to-air heat and moisture exchangers on indoor humidity. *ASHRAE Transactions* 95(2): 461–474.

Besant RW and Simonson CJ (2003) Air-to-air exchangers. *ASHRAE Journal* 45(4): 42–50.

Boardman CR, Glass SV and Carll CG (2010) Estimating foundation water vapor release using a simple moisture balance and AIM-2: case study of a contemporary wood-frame house. In: *Proceedings of the thermal performance of the exterior envelopes of whole buildings XI international conference*, Clearwater Beach, FL, 5–9 December 2010.

Carll CG, Boardman CR and Olson CL (2010) Case study: performance of a house built on a treated wood foundations system in a cold climate. In: *Proceedings of the thermal performance of the exterior envelopes of whole buildings XI international conference*, Clearwater Beach, FL, 5–9 December 2010.

Chen CC and Morey RV (1989) Comparison of four EMC/ERH equations. *Transactions of the American Society of Agricultural Engineers* 32(3): 983–990.

CSA (2009) *CAN/CSA-C439-09—Standard Laboratory Methods of Test for Rating the Performance of Heat/Energy-Recovery Ventilators*. Toronto, ON, Canada: CSA Group.

Fang X, Winkler J and Christensen D (2011) Using EnergyPlus to perform dehumidification analysis on Building America homes. *HVAC&R Research* 17(3): 268–283.

Home Ventilating Institute (HVI) (2012) *HVI-Certified Products Directory*. Wauconda, IL. Available at: http://www.hvi.org/proddirectory/HVICPD_Sec3_1Sept2012.pdf

Incropera F, Dewitt D, Bergman T, et al. (2006) *Fundamentals of Heat and Mass Transfer*. 6th ed. Hoboken, NJ: John Wiley & Sons.

Janssen H (2011) Thermal diffusion of water vapour in porous materials: fact or fiction? *International Journal of Heat and Mass Transfer* 54: 1548–1562.

Koutsoyiannis D (2012) Clausius-Clapeyron equation and saturation vapour pressure: simple theory reconciled with practice. *European Journal of Physics* 33: 295–305.

Niu JL and Zhang LZ (2001) Membrane-based enthalpy exchanger: material considerations and clarification of moisture resistance. *Journal of Membrane Science* 189: 179–191.

Oswin CR (1946) The kinetics of package life. III. The isotherm. *Journal of the Society of Chemical Industry* 65(12): 419–421.

Rode C and Woloszyn M (2007) Whole-building hygrothermal modeling in IEA Annex 41. In: *Proceedings of the thermal performance of the exterior envelopes of whole buildings X international conference*, Clearwater Beach, FL, 2–7 December 2007.

Schirmer R (1938) Die Diffusionszahl von Wasserdampf-Luft-Gemischen und die Verdampfungsgeschwindigkeit. *Beiheft VDI-Zeitschrift, Verfahrenstechnik* 6: 170–177.

Siau JF (1995) *Wood: Influence of Moisture on Physical Properties*. Blacksburg, VA: Department of Wood Science and Forest Products, Virginia Polytechnic Institute and State University.

Sparrow EM, Abraham JP, Martin GP, et al. (2001) An experimental investigation of a mass exchanger for transferring water vapor and inhibiting the transfer of other gases. *International Journal of Heat and Mass Transfer* 44: 4313–4321.

Stamm AJ (1964) *Wood and Cellulose Science*. New York: The Ronald Press Co.

Straube J and Burnett E (2005) *Building Science for Building Enclosures*. Westford, MA: Building Science Press.

Tanaka O (1984) An analysis of simultaneous heat and water vapor exchange through a flat paper plate cross flow total heat exchanger. *International Journal of Heat and Mass Transfer* 27(12): 2259–2265.

Walker IS and Sherman MH (2007) Humidity implications for meeting residential ventilation requirements. In: *Proceedings of the thermal performance of the exterior envelopes of whole buildings X international conference*, Clearwater Beach, FL, 2–7 December 2007.

Zhang LZ and Jiang Y (1999) Heat and mass transfer in a membrane-based energy recovery ventilator. *Journal of Membrane Science* 163: 29–38.

Appendix 1

Notation

A	area (m^2)
A_h	static component of convective heat transfer coefficient ($W\ m^{-2}\ K^{-1}$)
A_m	static component of convective moisture transfer coefficient ($kg\ m^{-2}\ s^{-1}\ Pa^{-1}$)
B_h	dynamic component of convective heat transfer coefficient ($W\ m^{-3}\ s\ K^{-1}$)
B_m	dynamic component of convective moisture transfer coefficient ($kg\ m^{-3}\ Pa^{-1}$)
c_b	bound water concentration ($kg\ m^{-3}$)
c_p	specific heat of dry air ($1006\ J\ kg^{-1}\ K^{-1}$)
c_v	water vapor concentration ($kg\ m^{-3}$)
C	sorption isotherm shape parameter, equation (11) (dimensionless)
d	membrane thickness (m)

d_c	characteristic length (m)
D_0	bound water diffusion coefficient at infinite temperature ($m^2\ s^{-1}$)
D_b	bound water diffusion coefficient ($m^2\ s^{-1}$)
D_u	moisture conductivity constant with moisture content as driving potential ($kg\ m^{-1}\ s^{-1}$)
D_v	water vapor diffusion coefficient ($m^2\ s^{-1}$)
D_{va}	water vapor diffusion coefficient in still air ($m^2\ s^{-1}$)
E_b	activation energy for bound water diffusion ($J\ mol^{-1}$)
$E_{i,j}$	node for exhaust air
h	relative humidity (dimensionless)
h_h	convective heat transfer coefficient ($W\ m^{-2}\ K^{-1}$)
h_m	convective mass transfer coefficient ($kg\ m^{-2}\ s^{-1}\ Pa^{-1}$)
J_b	bound water flux ($kg\ m^{-2}\ s^{-1}$)
J_m	total moisture flux (water vapor and bound water) ($kg\ m^{-2}\ s^{-1}$)
J_v	water vapor flux ($kg\ m^{-2}\ s^{-1}$)
k	membrane thermal conductivity ($W\ m^{-1}\ K^{-1}$)
l	length of ERV supply air channel (m)
L	enthalpy of vaporization of water (latent heat) ($J\ kg^{-1}$)
Nu	Nusselt number (dimensionless)
p_s	water vapor partial pressure at saturation (Pa)
p_v	water vapor partial pressure (Pa)
P_0	standard atmospheric pressure (101,325 Pa)
P_{atm}	atmospheric pressure (Pa)
q	heat flux ($W\ m^{-2}$)
R	universal gas constant ($8.314\ J\ mol^{-1}\ K^{-1}$)
R_v	specific gas constant for water vapor ($461.5\ J\ kg^{-1}\ K^{-1}$)
s	velocity of air through channels in ERV membrane ($m\ s^{-1}$)
$S_{i,j}$	node for supply air
t	temperature (°C)
T	absolute temperature (K)
u	moisture content (ratio of mass of water to mass of dry material) ($kg\ kg^{-1}$)
u_{max}	sorption isotherm parameter, equation (11): moisture content at 100% relative humidity ($kg\ kg^{-1}$)
w	humidity ratio (ratio of mass of water vapor to mass of dry air) ($kg\ kg^{-1}$)
x	spatial coordinate in the supply airflow direction (m)
y	spatial coordinate in the exhaust airflow direction (m)
z	spatial coordinate through the thickness of the membrane (m)
Z_h	resistance to heat flow ($m^2\ K\ W^{-1}$)
Z_m	resistance to moisture flow ($m^2\ s\ Pa\ kg^{-1}$)
δ_b	bound water permeability with vapor pressure as driving potential ($kg\ m^{-1}\ s^{-1}\ Pa^{-1}$)
δ_{meas}	experimental moisture permeability with vapor pressure as driving potential ($kg\ m^{-1}\ s^{-1}\ Pa^{-1}$)
δ_v	water vapor permeability with vapor pressure as driving potential ($kg\ m^{-1}\ s^{-1}\ Pa^{-1}$)
ε	moisture transfer (latent) effectiveness (dimensionless)
ρ	density of air ($kg\ m^{-3}$)

ρ_0	membrane dry density (kg m^{-3})
τ	tortuosity (dimensionless)
φ	porosity (fraction of total volume that is void) (dimensionless)
ψ	coefficient of moisture diffusion resistance (dimensionless)

Appendix 2

Estimating measurement error in membrane moisture permeability

The measured moisture permeability δ_{meas} (kg m^{-1} s^{-1} Pa^{-1}), which includes both vapor and bound water diffusion, is calculated as

$$\delta_{meas} = \frac{d}{\frac{A \cdot p_s \cdot \Delta h}{\dot{m}} - Z_m} \tag{27}$$

where d is the specimen thickness (m), A is the exposed surface area of the specimen (m^2), p_s is the saturation vapor pressure (Pa), Δh is the difference in relative humidity (RH) across the specimen (dimensionless), $\dot{m}$ is the rate of water vapor transmission through the specimen (kg s^{-1}), and Z_m is the resistance to water vapor transfer due to the air boundary layers at both surfaces of the specimen (m^2 s Pa kg^{-1}).

The membrane thickness has some inherent variability. A set of approximately 40 measurements gave a mean of 20 μm with a standard deviation of 2 μm or an uncertainty of ±10%.

The specimen surface area is known precisely; however, there is variability in the area occupied by the remnants of the structural spacer plates and glue lines. The membrane itself is estimated to occupy 75% ± 15% of the specimen area.

The error in saturation vapor pressure, based on temperature measurement error, is approximately ±1%. RH sensor error is ±0.01 for $h < 0.9$ and ±0.02 for $h \geq 0.9$.

The error in the measured rate of moisture transfer through the specimen is minimal. However, this rate must be corrected for the small rate of leakage through the edge of the specimen, which is measured independently with the permeation cell lid being covered with aluminum foil. The effective error depends on the relative rates of transmission through the specimen and edge leakage, varying between 5% and 25% under different conditions.

The boundary layer mass transfer resistance is measured in two ways. First, it is calculated from the moisture transfer rate with no specimen in the permeation cell under a range of RH conditions. Second, the moisture transfer rate is determined with one, two, and three layers of a nonhygroscopic membrane; the boundary layer resistance is calculated by extrapolation. Multiple measurements with both methods yield a total resistance at both surfaces of $Z_m = (6.6 \pm 0.4) \times 10^7$ m^2 s Pa kg^{-1}.

Errors in each parameter discussed above are propagated to give an estimated error in δ_{meas} at three sample conditions as shown in Figure 16.